

One-Pot Super Critical Fluid Synthesis of Spinel $MnFe_2O_4$ Nanoparticles and its Application as Anode Material for Mg-ion Battery

VINAY GANGARAJU^{1,✉}, TATHAGATA SARDAR^{1,✉}, KUNAL ROY^{1,✉}, MAHESH SHASTRI^{1,2,✉}, MANJUNATH SHETTY^{1,3,✉}, MURTHY MUNIYAPPA^{1,2,✉}, HIROAKI KOBAYASHI^{4,✉}, TAKAAKI TOMAI^{4,✉}, ANANDA KUMAR C S^{1,✉}, PRASANNA D. SHIVARAMU^{1,✉} and DINESH RANGAPPA^{1,✉}

¹Department of Applied Sciences (Nanotechnology), Centre for Post-Graduation Studies, Visvesvaraya Technological University, Muddenahalli Campus, Chikkaballapura-562101, India

²Department of Electronics & Communication, Nagarjuna College of Engineering & Technology, Devanahalli, Bengaluru-562164, India

³Department of Aeronautical and Automobile Engineering, Manipal Institute of Technology, Manipal-576104, India

⁴Institute of Multidisciplinary Research for Advanced Materials, Tohoku University, Sendai 980- 8577, Japan

*Corresponding authors: E-mail: dineshrangappa@gmail.com; prasuds@gmail.com

Received: 29 November 2021;

Accepted: 30 January 2022;

Published online: 10 March 2022;

AJC-20744

In present study, the synthesis of spinel $MnFe_2O_4$ nanoparticles using a facile one-pot super critical fluid method and their application for Mg-ion battery application as anode materials is reported. The synthesized $MnFe_2O_4$ nanoparticles were well characterized for their structure and morphology using XRD, SEM, TEM and EDS analysis. The average particle size of materials was less than 50 nm with spinel structure. The main feature of magnesium ion battery is its high specific capacity and large volumetric energy density, which makes it a promising alternative to Li-ion batteries. The spinel $MnFe_2O_4$ material has been used as an anode material for Mg-ion batteries. At different C-rates (0.05C to 2C), electrochemical charge-discharge behaviour has been observed. In first cycle of the phase-pure spinel structured anode, an initial specific capacity of 195.82 mAh/g, 139.70 mAh/g, 25.04 mAh/g and 14.16 mAh/g were obtained at C rate of 0.05C, 0.1C, 1C and 2C, respectively. A possible phase conversion reaction of the anode resulted in a decrease in specific capacity with increasing C-rate.

Keywords: Mg-ion battery, Spinel $MnFe_2O_4$, Anode, Conversion reaction, Charge-discharge performance.

INTRODUCTION

Over the last few years, chemical and electrochemical studies have increasingly focused on the development of novel rechargeable batteries as an energy storage alternative to lithium ion batteries [1-6]. Other than the rechargeable Li-ion battery, Mg-ion batteries are receiving much attention due to their natural abundance, safety, high specific capacity of around 2205 Ah kg^{-1} and high volumetric energy density of 3833 mAh cm^{-3} [7-9]. Due to its divalence it can lead to a phenomenally large theoretical capacity by the redox reaction between Mg and Mg^{2+} [10]. In spite of this, there is no much significant advancements in the field of multivalent magnesium ion batteries compared to lithium ion batteries because of two factors: (a) the kinetics of intercalation and diffusion of Mg ions within the host lattice and (b) the discordance of a high electrolytic window with the metal anode and high voltage cathodes [11-13].

So far, intercalation of cathodes has been used with comparatively low capacities and cell potentials, in addition to the fact that their capacity declines significantly over a period. In these cases, the main cause is the slow diffusion of Mg^{2+} ions that results in ion adsorption on the electrode due to polarization of the electrode. In addition, a co-intercalation of solvent molecules results in structural destruction and degeneration of the cathode material and instability of the intercalates. Another problem which affects cell performance efficiency is the formation of passivation layers in solid-electrolyte interfaces (SEI), which creates a barrier to Mg^{2+} transport. Therefore, future research focuses on improving the efficiency of cells mainly by changing the structure of intercalation and conversion electrodes [5]. Since $MnFe_2O_4$ spinel structured oxide does not reduce during the discharge process of a cell, it may be used to fabricate electrodes in Mg ion batteries with an 80.4 mAh g^{-1} capacity [14-20].

Metal sulfides with Chevral phase such as Mo_6S_8 have been extensively studied as cathode materials for magnesium batteries [7]. Although their terminal voltage is low (1.0-1.2 V), they are not the ideal material for future electrodes. Despite their potential high energy density, some metal oxides (like V_2O_5 , MoO_3 , MnO_2 , *etc.*) have low rate capability due to their slow ion diffusion [21]. The high dielectric constant of spinel metal oxides (AB_2O_4) have generated a lot of interest in discussions about ion diffusivity [22,23]. Recent research has explored spinel metal oxides for Li-ion batteries, magnesium ion batteries and nickel-ion batteries; however, these materials have not been adequately explored for use as anode materials. Recently, Yokozaki *et al.* [24] reported that spinel MgMn_2O_4 can exhibit a theoretical capacity of 540 mAh g^{-1} for both $\text{Mn}^{3+}/\text{Mn}^{4+}$ and $\text{Mn}^{3+}/\text{Mn}^{2+}$ redox transformations. During lithium intercalation, Thackeray *et al.* [25,26] synthesized LiMn_2O_4 as a cathode and showed excellent electrochemical performance at low voltage (*vs.* Li metals). It has also been shown that spinel's can have their properties tuned by replacing or substituting Mn with Ni, Co or Cr to increase the voltage up to 5.0 V [27-30].

Mg-ion batteries have been investigated for the development of their electrode materials for the past two decades. For the development of electrode materials, various spinel metal oxides, including MgM_2O_4 ($\text{M} = \text{Mn, Fe, Ni, Co, etc.}$) are being studied. According to Truong *et al.* [2,31,32], spinel MgMn_2O_4 (with a capacity of 270 mAh g^{-1}) and MgCo_2O_4 (with a capacity of 124 mAh g^{-1}) have been extensively studied as cathode materials for Mg-ion batteries with capacities of 69.8 mAh g^{-1} . Bock *et al.* [17] studied several spinel ferrites from the molecular and theoretical aspects, including Fe_3O_4 , ZnFe_2O_4 and MgFe_2O_4 and found that different vacancies in the divalent cation of the spinel ferrite can lead to differences in the deformation and delivered capacity of the spinel ferrite.

In view of the above, the above-mentioned material shares a lot of characteristics with MgCo_2O_4 and MgMn_2O_4 (efficient cathode materials for Mg ion batteries, as reported by Truong *et al.* [31,32]). Our research team designed and analyzed the performance of spinel MnFe_2O_4 as an emerging anode material for Mg ion batteries considering these findings [3]. These simple and efficient hydrothermal, solvothermal and super critical fluid processes are of great interest, as the particle size and morphology that are desired can be controlled [34,35]. Furthermore, there have been no reports to date on the one-pot synthesis using super critical fluid process for MnFe_2O_4 as the anode material in Mg ion batteries. Thus, MnFe_2O_4 nanoparticles have been synthesized using a one pot super critical fluid process method in the present investigation. This work also makes it possible for MnFe_2O_4 anode to be applied in a rechargeable Mg ion battery for the first time by studying conversion reaction phenomena in parallel.

EXPERIMENTAL

The chemicals *viz.* $\text{FeCl}_3 \cdot 6\text{H}_2\text{O}$ and $\text{Mn}(\text{NO}_3)_2 \cdot 6\text{H}_2\text{O}$ (Lobachemie Laboratory Reagents & Fine Chemicals) were procured for the synthesis of MnFe_2O_4 nanoparticles. Sodium hydroxide (ChemLabs) and sodium dodecyl sulfate (SDS, Merck) were used as reducing and capping agents, respectively. Ethylene

glycol (SD Fine Chemicals Ltd.) was used as a solvent. All the chemicals are of analytical grade unless mentioned.

Synthesis of MnFe_2O_4 nanoparticles by one-pot super-critical fluid process: MnFe_2O_4 nanoparticles were synthesized using $\text{Mn}(\text{NO}_3)_2 \cdot 6\text{H}_2\text{O}$ and $\text{FeCl}_3 \cdot 6\text{H}_2\text{O}$ as precursor salts in 2:1 stoichiometric ratios (Mn:Fe). Ethylene glycol (10 mL) was added to the precursor materials and mixture was stirred for 1 h and 3.5 M NaOH was added to get hydrated manganese nitrate and ferric chloride. Following NaOH addition, 21 mM of SDS was added and stirred for 1 h. Then, the solution was transferred to stainless steel super critical reactor and kept in muffle furnace at 480°C for 20 min. To remove the impurities, the precipitated part was washed several times with deionized water and ethanol after heat treatment. This was followed by 6 h of vacuum drying at 60°C .

Electrode fabrication: Electrochemical performance of the synthesized MnFe_2O_4 nanoparticles as electrode materials was studied using CR2032 coin cells. Anode material (MnFe_2O_4) was combined with the PVDF binder and acetylene black (as conductive material) in the ratio of 8:1:1 (based on weight %), to fabricate the working electrode. All the three materials were grounded using mortar and pestle followed by the addition of *N*-methyl 2-pyrrolidone to prepare electrode paste. Thus, prepared paste was coated uniformly on the copper sheet and allowed to dry overnight at 80°C . Dried sheets were cut into circular discs after to use as anodes. Similarly, Mg metal as the reference electrode, which was also cut into same circular discs as that of anode. The cell was assembled in a Ar-filled glove box. Polypropylene film (thickness 20-25 mm) was used as a separator between cathode and anode and the electrolyte used was 0.5 M of $\text{Mg}(\text{ClO}_4)_2$ in acetonitrile. A multichannel battery tester (Arbin Workstation) was then used to measure the charge-discharge cycling performance of the fabricated cells.

Characterization: To determine the structure of synthesized powder, powder X-ray diffractometer (RigakuUltima 4 at 40 kV and 30 mA) was used to irradiate $\text{CuK}\alpha$ with a wavelength of 1.54 \AA . Using a 2θ diffraction angle, data were collected with a step size of 0.02° and the following equation was used to calculate the crystallite size of the average:

$$D_{\text{avg}} = \frac{0.9\lambda}{\beta \cos \theta} \quad (1)$$

Here, λ is the wavelength of X-ray (1.54060 \AA), β is the width at half maximum (FWHM) and θ is the angle of diffraction. SEM (Hitachi 150) was used to study the morphology of the synthesized powder. SEM attached energy-dispersive spectroscopy (EDS) analysis of the synthesized powder was used to determine the powder's composition. Transmission electron microscopy (TEM, Hitachi) data of the as-prepared sample were obtained. An electrochemical charge-discharge measurement was performed on the sample using Arbin electrochemical workstation.

RESULTS AND DISCUSSION

A spinel (AB_2O_4) is classified as either normal or inverse, depending on the distribution of cations within the crystal

lattice. Usually, cubic systems with close packing can be found in normal spinel's. According to crystal field stabilization theory (CFST), all A-cations occupy octahedral sites in inverse spinel's, whereas half of the B-cations do so, as A-cations have a strong preferential effect on octahedral sites [36,37]. The XRD pattern of as-synthesized MnFe_2O_4 was recorded and displayed in Fig. 1. As evidenced by XRD, the pattern corresponded to inverse cubic spinel structure of space group $\text{Fd}\bar{3}\text{m}$. XRD pattern characterization software provided the following cell parameters: $a = b = c = 8.50 \text{ \AA}$ and $\alpha = \beta = \gamma = 90^\circ$. The parameters of these cells are in good agreement with the previous reports [38]. There is a major characteristic peak of ferrite spinel located at lattice plane (3 1 1) and they have existed for a long time based on this evidence [39]. Earlier reporters also made similar observations [40,41]. In the sample, there were no residual phases of $\alpha\text{-Fe}_2\text{O}_3$ or other impurities. Based on Scherrer's formula (eqn. 1), the average crystallite size of MnFe_2O_4 is 11.93 nm, which corresponds to the lattice planes (1 1 1), (2 2 0), (3 1 1), (2 2 2), (4 0 0), (4 2 2), (5 1 1) and (4 4 0).

Fig. 2a-b shows SEM micrographs of nano- MnFe_2O_4 powder, which illustrate the morphology of the particles. As it can be seen in the SEM image that the particles are spherical

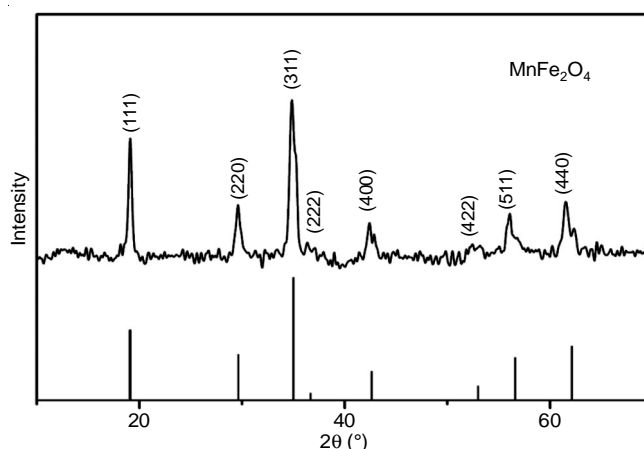


Fig. 1. XRD pattern of MnFe_2O_4 synthesized by one-pot supercritical fluid process

in shape and agglomerated. TEM images in Fig. 2c-d clearly show agglomerated spherical particles and are of the size less than size of 50 nm. TEM images provide a glimpse into the particle morphology and size distribution, as the particles have almost uniform morphology and size distribution.

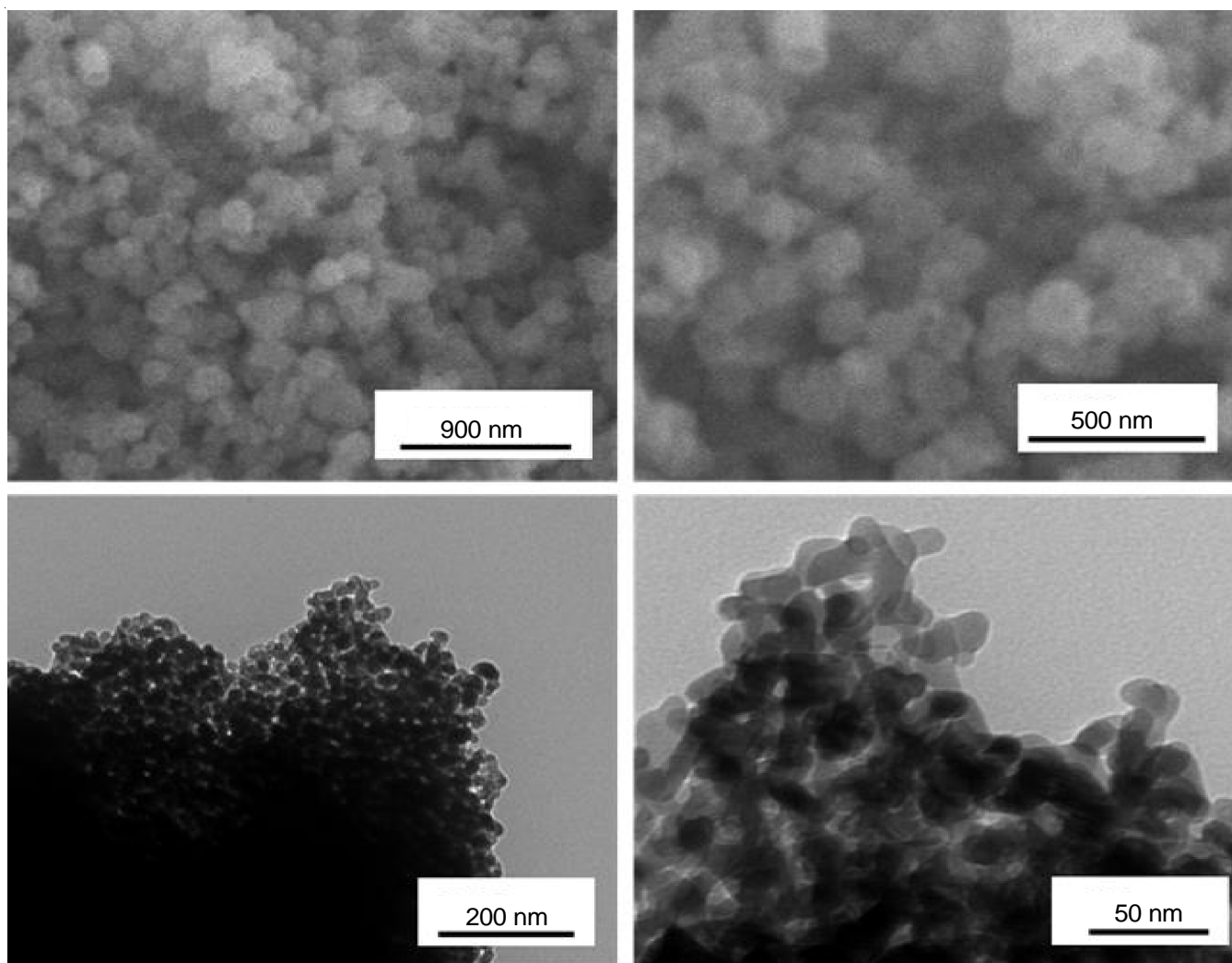


Fig. 2. (a,b) SEM image and (c,d) TEM images of MnFe_2O_4 nanoparticles synthesized by one-pot supercritical fluid method

A further study has been conducted to determine the elemental composition and phase purity of synthesized ferrite with EDS spectral analysis. Fig. 3 clearly shows the presence of regular Mn, Fe, O characteristic peaks with pure MnFe_2O_4 phase. The EDS analysis also provided an estimation of the elemental composition based on the composition mixed when the sample was prepared.

In synthesized samples, the XPS study provides quantitative information on compositional variance and metal ions oxidation state (oxidation state). It is possible to consider the occurrence of C 1s as the result of hydrocarbon contamination with other elements [39]. In Fig. 4b, Mn 2p represents split-spin orbit components $2p_{3/2}$ and $2p_{1/2}$ significantly at 634.817 and 645.94 eV, respectively. In Fig. 4c, Fe 2p exhibits split-

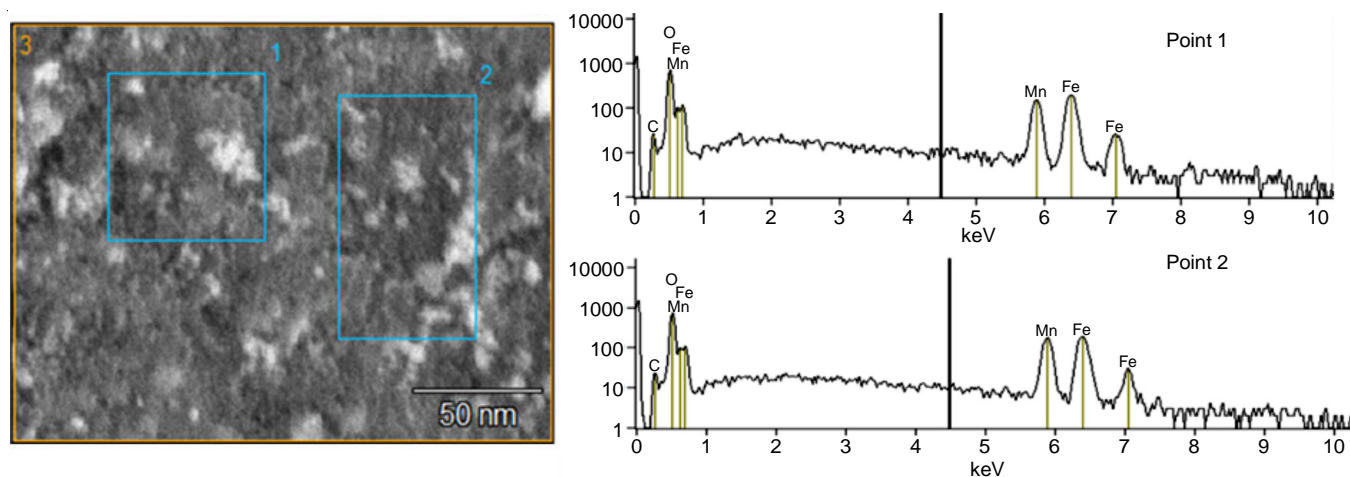


Fig. 3. EDS spectra with SEM image on C-substrate

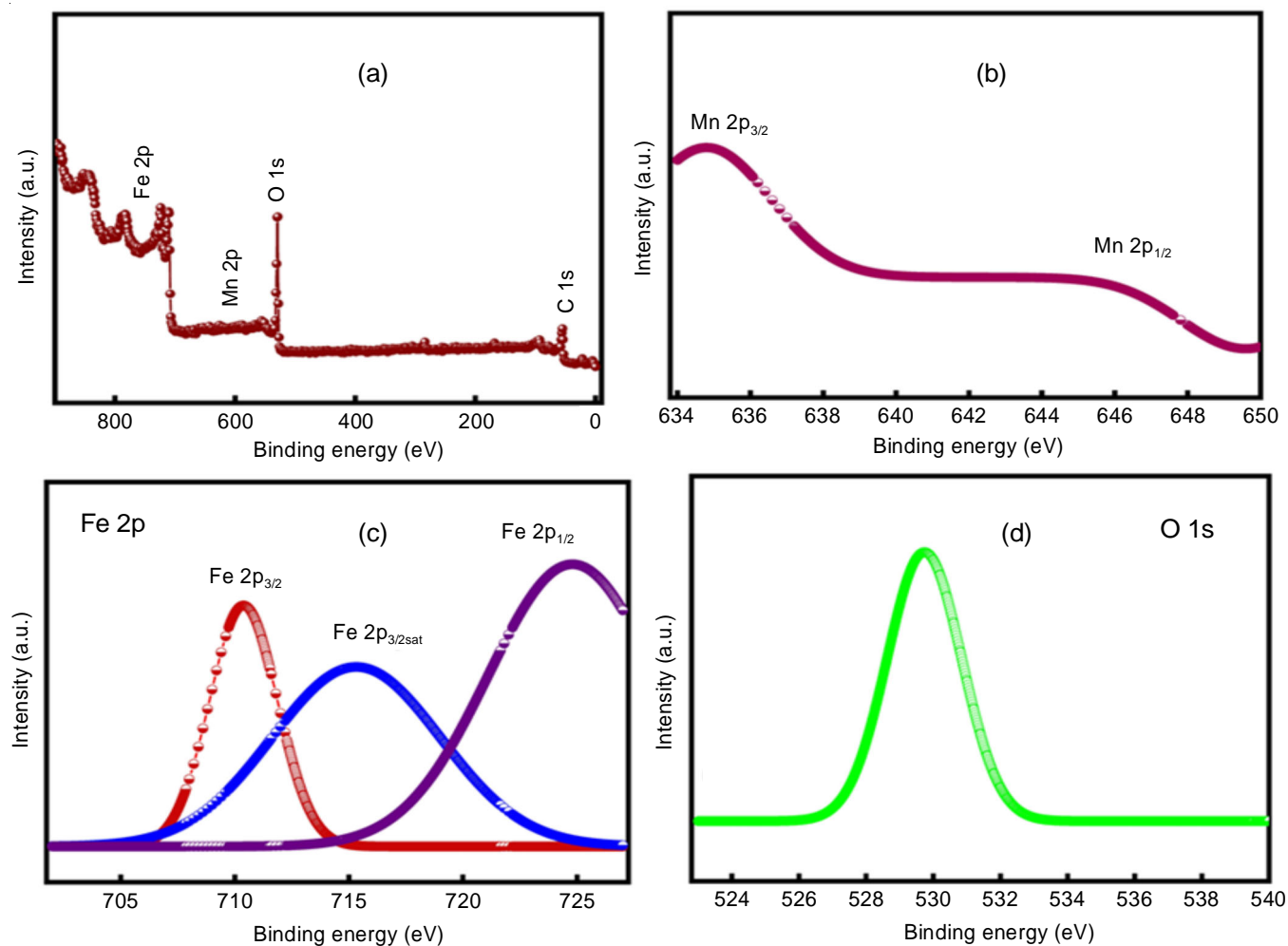
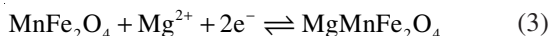
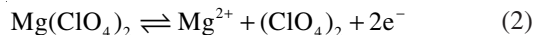


Fig. 4. (a) XPS survey scan of as-prepared MnFe_2O_4 ; (b-d) High resolution XPS scan for Fe 2p, Mg 1s and O 1s core levels, respectively

spin orbits $2p_{3/2}$ and $2p_{1/2}$ significantly at 710.355 and 725.09 eV, respectively. At the binding energy of 529.731 eV, Fig. 4d indicates the presence of O 1s.

Electrochemical charge discharge: During the conversion reaction between spinel and rock-salt frame, the magneziation-demagneziation process drives the storage mechanism of electrode material (MnFe₂O₄).



Anode materials for Mg ion batteries such as MnFe₂O₄ were investigated *via* galvanostatic charge/discharge within a voltage range between -1.0 V and 1.0 V vs. C. As can be seen in Fig. 5, the MnFe₂O₄ charge-discharge profiles were typical of a first cycle of using different C-rates. There was, however, a rapid decrease of the voltage window from 1.0 V to -0.5 V in the discharge profiles. This may have been due to the change of MnFe₂O₄ from spinel to rock-salt framework through Mg-insertion or magneziation into the anode. Similarly, the voltage window dropped slowly from -0.5 V to -1.0 V and discharge capacities of 195.82, 139.70, 25.04 and 14.16 mAh/g were observed, with increasing C-rate the capacity decreases. This implies a surface reaction on the cathode or electrolyte decomposition due to increased volume expansion/contraction in the lattice structure of the anode [32,42]. In the rock-salt phase, the high charge capacities are attributed to the Mg-insertion into spinel structure [23,43-47].

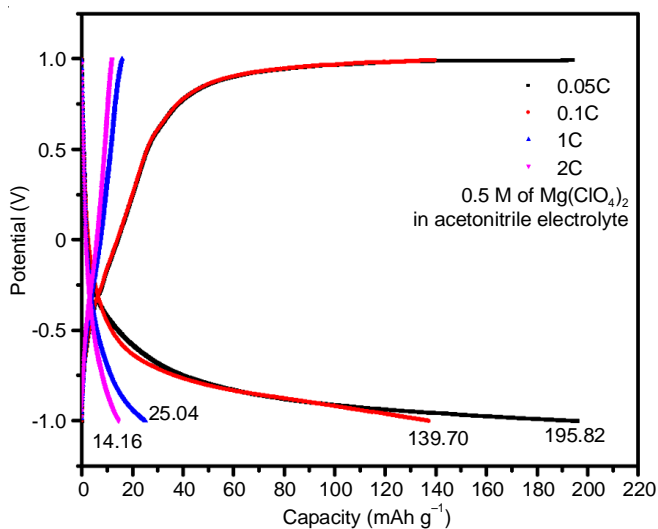


Fig. 5. Charge-discharge profile of MnFe₂O₄ at 0.05C, 0.1C, 1C, 2C current density

With discharge profiles at 0.05C and 0.1C found an irreversible capacity loss was observed due to lattice distortion in the anode caused by magneziation-demagneziation with a wide potential plateau near -0.75V. As compared to the other cases, the discharge plateau has been shifted to -1.0 V and narrowed at 1C and 2C with less irreversible capacity loss.

Conclusion

A single-phase MnFe₂O₄ nanocrystals were achieved successfully synthesized by a one-pot procedure. Due to the uniform

morphology and high electrolyte-ions interfacial contact, its applicability as an emerging electrode material for rechargeable Mg ion batteries has been elucidated. Herein, MnFe₂O₄ was used as an anode here, following the principle of the conversion type electrode by participating in large volume expansion reactions phenomena, which allowed ion diffusion into the crystalline structure as well as structural distortion at the same time. It showed a discharge capacity of 195.82 mAh/g at 0.05C, simultaneously 139.70 mAh/g, 25.04 mAh/g and 14.16 mAh/g at a C rate of 0.1C, 1C and 2C were obtained, respectively. Further, MnFe₂O₄ may decompose at higher current rates, so the specific capacity decreased to 14.16 mAh g⁻¹ at 2C as the current rate increased.

ACKNOWLEDGEMENTS

The authors acknowledge the support given by Department of Science & Technology International Bilateral Cooperation Division, Government of India (Grant No. DST/INT/JSPS/P-270/2018).

CONFLICT OF INTEREST

The authors declare that there is no conflict of interests regarding the publication of this article.

REFERENCES

1. Y. Liu, N. Zhang, C. Yu, L. Jiao and J. Chen, *Nano Lett.*, **16**, 3321 (2016); <https://doi.org/10.1021/acs.nanolett.6b00942>
2. Q.D. Truong, M. Kempaiah Devaraju, P.D. Tran, Y. Gambe, K. Nayuki, Y. Sasaki and I. Honma, *Chem. Mater.*, **29**, 6245 (2017); <https://doi.org/10.1021/acs.chemmater.7b01252>
3. M.-C. Lin, M. Gong, B. Lu, Y. Wu, D.-Y. Wang, M. Guan, M. Angell, C. Chen, J. Yang, B.-J. Hwang and H. Dai, *Nature*, **520**, 324 (2015); <https://doi.org/10.1038/nature14340>
4. A. Ponrouch, C. Frontera, F. Bardé and M.R. Palacín, *Nat. Mater.*, **15**, 169 (2016); <https://doi.org/10.1038/nmat4462>
5. J. Muldoon, C.B. Bucur and T. Gregory, *Chem. Rev.*, **114**, 11683 (2014); <https://doi.org/10.1021/cr500049y>
6. S. Tepavcevic, Y. Liu, D. Zhou, B. Lai, J. Maser, X. Zuo, H. Chan, P. Král, C.S. Johnson, V. Stamenkovic, N.M. Markovic and T. Rajh, *ACS Nano*, **9**, 8194 (2015); <https://doi.org/10.1021/acs.nano.5b02450>
7. D. Aurbach, Z. Lu, A. Schechter, Y. Gofer, H. Gizbar, R. Turgeman, Y. Cohen, M. Moshkovich and E. Levi, *Nature*, **407**, 724 (2000); <https://doi.org/10.1038/35037553>
8. L.F. Wan and D. Prendergast, *J. Am. Chem. Soc.*, **136**, 14456 (2014); <https://doi.org/10.1021/ja505967u>
9. T.J. Carter, R. Mohtadi, T.S. Arthur, F. Mizuno, R. Zhang, S. Shirai and J.W. Kampf, *Angew. Chem. Int. Ed.*, **53**, 3173 (2014); <https://doi.org/10.1002/anie.201310317>
10. P. Novák, R. Imhof and O. Haas, *Electrochim. Acta*, **45**, 351 (1999); [https://doi.org/10.1016/S0013-4686\(99\)00216-9](https://doi.org/10.1016/S0013-4686(99)00216-9)
11. J. Muldoon, C.B. Bucur, A.G. Oliver, T. Sugimoto, M. Matsui, H.S. Kim, G.D. Allred, J. Zajicek and Y. Kotani, *Energy Environ. Sci.*, **5**, 5941 (2012); <https://doi.org/10.1039/c2ee03029b>
12. E. Levi, Y. Gofer and D. Aurbach, *Chem. Mater.*, **22**, 860 (2010); <https://doi.org/10.1021/cm9016497>
13. Z. Lu, A. Schechter, M. Moshkovich and D. Aurbach, *J. Electroanal. Chem.*, **466**, 203 (1999); [https://doi.org/10.1016/S0022-0728\(99\)00146-1](https://doi.org/10.1016/S0022-0728(99)00146-1)
14. P. Poizot, S. Laruelle, S. Grugeon, L. Dupont and J.-M. Tarascon, *Nature*, **407**, 496 (2000); <https://doi.org/10.1038/35035045>

15. Y. Pan, Y. Zhang, X. Wei, C. Yuan, J. Yin, D. Cao and G. Wang, *Electrochim. Acta*, **109**, 89 (2013); <https://doi.org/10.1016/j.electacta.2013.07.026>
16. N. Sivakumar, S.R.P. Gnanakan, K. Karthikeyan, S. Amaresh, W.S. Yoon, G.J. Park and Y.S. Lee, *J. Alloys Compd.*, **509**, 7038 (2011); <https://doi.org/10.1016/j.jallcom.2011.03.123>
17. D.C. Bock, K.R. Tallman, H. Guo, C. Quilty, S. Yan, P.F. Smith, B. Zhang, D.M. Lutz, A.H. McCarthy, M.M. Huie, V. Burnett, A.M. Bruck, A.C. Marschilok, E.S. Takeuchi, P. Liu and K.J. Takeuchi, *Phys. Chem. Chem. Phys.*, **22**, 26200 (2020); <https://doi.org/10.1039/D0CP02322A>
18. C. Kim, P.J. Phillips, B. Key, T. Yi, D. Nordlund, Y.-S. Yu, R.D. Bayliss, S.-D. Han, M. He, Z. Zhang, A.K. Burrell, R.F. Klie and J. Cabana, *Adv. Mater.*, **27**, 3377 (2015); <https://doi.org/10.1002/adma.201500083>
19. M. Liu, Z. Rong, R. Malik, P. Canepa, A. Jain, G. Ceder and K.A. Persson, *Energy Environ. Sci.*, **8**, 964 (2015); <https://doi.org/10.1039/C4EE03389B>
20. Z. Feng, X. Chen, L. Qiao, A.L. Lipson, T.T. Fister, L. Zeng, C. Kim, T. Yi, N. Sa, D.L. Proffitt, A.K. Burrell, J. Cabana, B.J. Ingram, M.D. Biegalski, M.J. Bedzyk and P. Fenter, *ACS Appl. Mater. Interfaces*, **7**, 28438 (2015); <https://doi.org/10.1021/acsami.5b09346>
21. H.D. Yoo, I. Shterenberg, Y. Gofer, G. Gershinsky, N. Pour and D. Aurbach, *Energy Environ. Sci.*, **6**, 2265 (2013); <https://doi.org/10.1039/c3ee40871j>
22. M. Mao, T. Gao, S. Hou and C. Wang, *Chem. Soc. Rev.*, **47**, 8804 (2018); <https://doi.org/10.1039/C8CS00319J>
23. S. Okamoto, T. Ichitsubo, T. Kawaguchi, Y. Kumagai, F. Oba, S. Yagi, K. Shimokawa, N. Goto, T. Doi and E. Matsubara, *Adv. Sci.*, **8**, 1500072 (2015); <https://doi.org/10.1002/advs.201500072>
24. R. Yokozaki, H. Kobayashi and I. Honma, *Ceram. Int.*, **47**, 10236 (2021); <https://doi.org/10.1016/j.ceramint.2020.10.184>
25. M.M. Thackeray, W.I.F. David, P.G. Bruce and J.B. Goodenough, *Mater. Res. Bull.*, **18**, 461 (1983); [https://doi.org/10.1016/0025-5408\(83\)90138-1](https://doi.org/10.1016/0025-5408(83)90138-1)
26. M.M. Thackeray, *Prog. Solid State Chem.*, **25**, 1 (1997); [https://doi.org/10.1016/S0079-6786\(97\)81003-5](https://doi.org/10.1016/S0079-6786(97)81003-5)
27. K. Amine, H. Tukamoto, H. Yasuda and Y. Fujita, *J. Electrochem. Soc.*, **143**, 1607 (1996); <https://doi.org/10.1149/1.1836686>
28. Y. Terada, K. Yasaka, F. Nishikawa, T. Konishi, M. Yoshio and I. Nakai, *J. Solid State Chem.*, **156**, 286 (2001); <https://doi.org/10.1006/jssc.2000.8990>
29. D. Liu, Y. Lu and J.B. Goodenough, *J. Electrochem. Soc.*, **157**, A1269 (2010); <https://doi.org/10.1149/1.3491365>
30. H. Kawai, M. Nagata, H. Kageyama, H. Tukamoto and A.R. West, *Electrochim. Acta*, **45**, 315 (1999); [https://doi.org/10.1016/S0013-4686\(99\)00213-3](https://doi.org/10.1016/S0013-4686(99)00213-3)
31. Q.D. Truong, H. Kobayashi, K. Nayuki, Y. Sasaki and I. Honma, *Solid State Ion.*, **344**, 115136 (2020); <https://doi.org/10.1016/j.ssi.2019.115136>
32. Q.D. Truong, H. Kobayashi and I. Honma, *RSC Adv.*, **9**, 36717 (2019); <https://doi.org/10.1039/C9RA04936C>
33. T.S. Arthur, R. Zhang, C. Ling, P.-A. Glans, X. Fan, J. Guo and F. Mizuno, *ACS Appl. Mater. Interfaces*, **6**, 7004 (2014); <https://doi.org/10.1021/am5015327>
34. M. Okubo, E. Hosono, J. Kim, M. Enomoto, N. Kojima, T. Kudo, H. Zhou and I. Honma, *J. Am. Chem. Soc.*, **129**, 7444 (2007); <https://doi.org/10.1021/ja0681927>
35. M. Okubo, Y. Mizuno, H. Yamada, J. Kim, E. Hosono, H. Zhou, T. Kudo and I. Honma, *ACS Nano*, **4**, 741 (2010); <https://doi.org/10.1021/nn9012065>
36. M. Fracchia, M. Manzoli, U. Anselmi-Tamburini and P. Ghigna, *Scr. Mater.*, **188**, 26 (2020); <https://doi.org/10.1016/j.scriptamat.2020.07.002>
37. V.S. Zhandun and A.V. Nemtsev, *Mater. Chem. Phys.*, **259**, 124065 (2021); <https://doi.org/10.1016/j.matchemphys.2020.124065>
38. A. Sankaramahalingam and J.B. Lawrence, *Nano-Metal Chem.*, **42**, 121 (2012); <https://doi.org/10.1080/15533174.2011.609500>
39. W.B. Cross, L. Affleck, M.V. Kuznetsov, I.P. Parkin and Q.A. Pankhurst, *J. Mater. Chem.*, **9**, 2545 (1999); <https://doi.org/10.1039/a904431k>
40. M.A. Ahmed, E. Ateia and F.M. Salem, *J. Mater. Sci.*, **42**, 3651 (2007); <https://doi.org/10.1007/s10853-006-1349-0>
41. F.A. Radwan, M.A. Ahmed and G. Abdelatif, *J. Phys. Chem. Solids*, **64**, 2465 (2003); <https://doi.org/10.1016/j.jpcs.2003.08.003>
42. K. Shimokawa and T. Ichitsubo, *Curr. Opin. Electrochem.*, **21**, 93 (2020); <https://doi.org/10.1016/j.coelec.2020.01.017>
43. N. Kitamura, Y. Tanabe, N. Ishida and Y. Idemoto, *Chem. Commun.*, **55**, 2517 (2019); <https://doi.org/10.1039/C8CC09713F>
44. K. Shimokawa, H. Matsumoto and T. Ichitsubo, *J. Phys. Chem. Lett.*, **9**, 4732 (2018); <https://doi.org/10.1021/acs.jpcllett.8b02209>
45. Y. Kotani, R. Ise, K. Ishii, T. Mandai, Y. Oaki, S. Yagi and H. Imai, *J. Alloys Compd.*, **739**, 793 (2018); <https://doi.org/10.1016/j.jallcom.2017.12.315>
46. T. Ichitsubo, S. Okamoto, T. Kawaguchi, Y. Kumagai, F. Oba, S. Yagi, N. Goto, T. Doi and E. Matsubara, *J. Mater. Chem. A Mater. Energy Sustain.*, **3**, 10188 (2015); <https://doi.org/10.1039/C5TA01365H>
47. T. Ichitsubo, T. Adachi, S. Yagi and T. Doi, *J. Mater. Chem.*, **21**, 11764 (2011); <https://doi.org/10.1039/c1jm11793a>